Structural and Functional Analysis of SAM-Dependent *N*-Methyltransferases Involved in Ovoselenol and Ovothiol Biosynthesis

Kendra A. Ireland,[1,4] Chase M. Kayrouz,[2,4] Marissa L. Abbott,[2] Mohammad R. Seyedsayamdost,[2,3] and Katherine M. Davis[1,*]

[1]Department of Chemistry, Emory University, Atlanta, GA 30322, United States

[2]Department of Chemistry, Princeton University, Princeton, NJ 08544, United States

[3]Department of Molecular Biology, Princeton University, Princeton, NJ 08544, United States

[4]These authors contributed equally

*Correspondence: katherine.davis@emory.edu, 404-712-6865, 1515 Dickey Drive, Emory University, Atlanta, GA 30322

ABSTRACT

Thio/selenoimidazole *N*π-methyltransferases are an emerging family of enzymes responsible for catalyzing the final enzymatic step in the biosynthesis of ovothiol and ovoselenol, S/Se-containing histidine-derived antioxidants. These unique enzymes are widespread among prokaryotes yet bear only marginal sequence similarity to other known methyltransferases. Likewise, little is known about the structural determinants of their reactivities. Here we report the first ligand-bound X-ray crystal structures of this family, including OvsM from the ovoselenol pathway as well as a member of a previously unknown clade of standalone ovothiol-biosynthetic *N*π-methyltransferases, which we have designated OvoM. Unlike previously reported ovothiol methyltransferases, which are fused as a *C*-terminal domain to the sulfoxide synthase OvoA, OvoMs are discrete enzymes and function independently. Comparative structural analyses of OvsM and OvoM reveal several conserved, ligand-induced tertiary and secondary structure changes, and suggest that similar conformational changes may apply to dual-domain OvoA enzymes. Mutagenesis experiments support a model in which the rearrangement of OvoA's two domains facilitates substrate recognition through interaction with a key Tyr residue located within the domain linker. Furthermore, biochemical experiments highlight the essential role of an active site Asp residue, which likely functions as a catalytic base in the S_N2-like nucleophilic substitution reaction catalyzed by these enzymes.

Main Text

INTRODUCTION

Thio/selenoimidazoles (TSIs) are S- and Se-containing biomolecules derived from histidine and synthesized by bacteria, fungi, and archaea (Fig. 1A).[1] Their antioxidant qualities play a crucial role in the oxidative stress responses of their producers and hold promise for the prevention and treatment of a spectrum of inflammatory conditions in humans.[2-6] TSIs characterized to date include ergothioneine and ovothiol, along with their Se isologs selenoneine and the recently identified molecule ovoselenol. Following its discovery, the biosynthetic pathway of ovoselenol was elucidated (Fig. 1B).[7] This pathway begins with the formation of *N*-acetyl-1-seleno-β-D-glucosamine (SeGlcNAc), catalyzed by homologs of the selenophosphate synthetase SenC and the selenosugar synthase SenB from the *sen* biosynthetic gene cluster.[8] Oxidative coupling of SeGlcNAc with histidine is then catalyzed by a member of the non-heme iron-dependent sulfoxide/selenoxide synthase (NHISS) family. This enzyme, OvsA, generates a selenoxide intermediate via the installation of a C–Se bond at the imidazole 5'-carbon of histidine. The selenoxide intermediate rapidly undergoes *syn* elimination to release the sugar moiety followed by reduction to afford 5-selenohistidine (5-SeHis). A final *S*-adenosylmethionine (SAM)-dependent methylation at the imidazole π-nitrogen of 5-SeHis, mediated by OvsM, completes the pathway to yield the mature natural product. While the biosynthesis of ovothiol proceeds similarly, the required NHISS and methyltransferase functionalities were reported to be integrated within the bifunctional enzyme OvoA.[9,10] Unlike OvsM, however, the methyltransferase domain of OvoA does not directly accept the product of its NHISS domain; instead, an additional lyase (OvoB) is needed to cleave the cysteinyl C–S bond prior to methylation (Fig. 1B).

Our recent crystal structures of SenB and OvsA offer insights into ligand recognition and associated conformational changes important for selenosugar biosynthesis, as well as elucidate the molecular basis for 5'-specific C–Se bond formation *en route* to ovoselenol.[7, 11] In this study, we further illuminate ovoselenol biosynthesis by providing structural insights into the final enzymatic transformation. While Wang et al. clarified the mode of ligand binding within the NHISS domain of a bifunctional OvoA from *Hydrogenimonas thermophila* ($OvoA_{Th2}$), the structure of the

methyltransferase domain was reported only in the apo state.[12] Herein, we present the first visualization of ligand binding by *Nπ*-methyltransferases involved in TSI biosynthesis. Structures of OvsM are reported, together with bioinformatic identification and structural characterization of a standalone *Nπ*-methyltransferase involved in ovothiol biosynthesis, which we have termed OvoM. Together with the published model of $OvoA_{Th2}$, these results enable a comparative structural analysis of the three methyltransferase classes involved in ovothiol and ovoselenol biosynthesis. Mutagenesis studies provide further insights into ligand recognition by the methyltransferase domain of bifunctional $OvoA_{Th2}$, as well as the reaction mechanism of these enzymes.

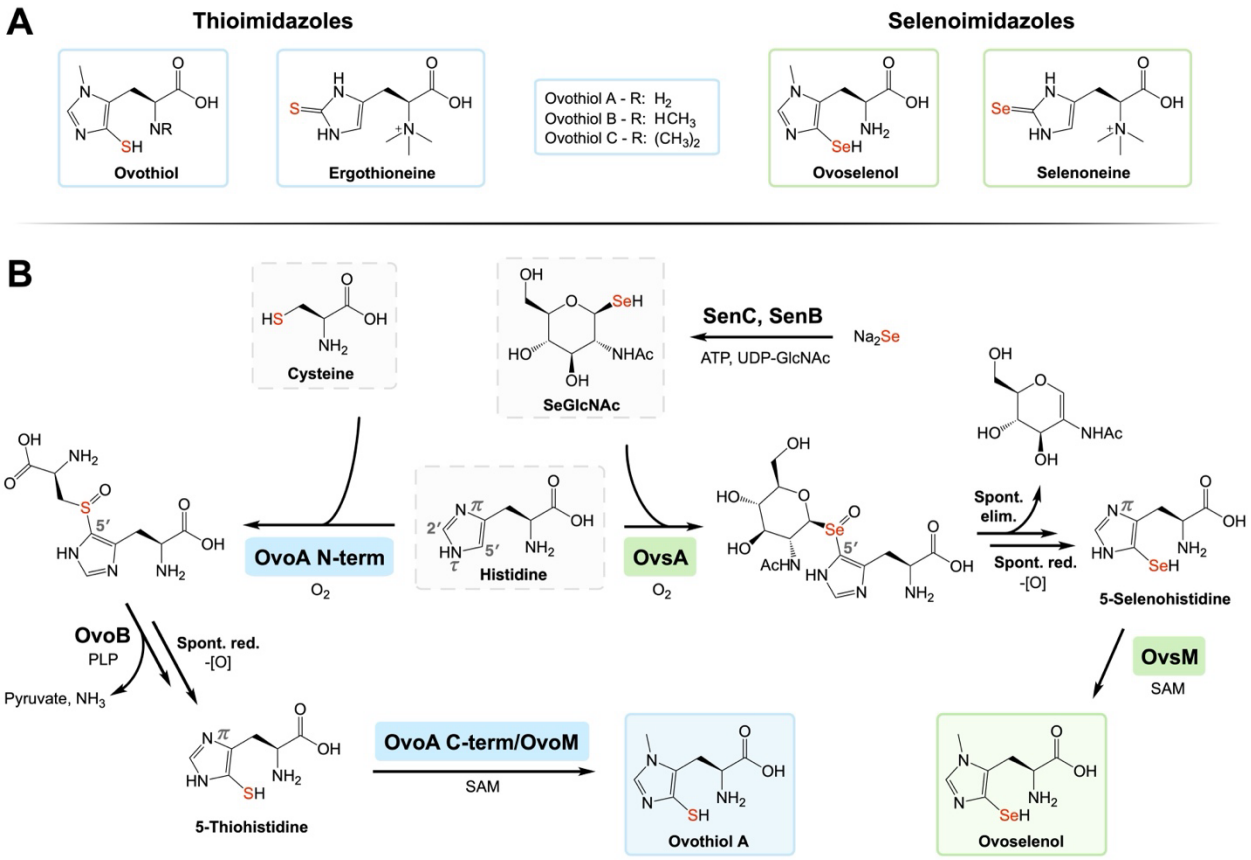

Figure 1. Thio/selenoimidazoles and associated biosynthetic pathways. (**A**) Structures of the four currently known TSIs. (**B**) Biosynthetic pathways for ovothiol and ovoselenol.

RESULTS AND DISCUSSION

Phylogenetic analysis reveals monofunctional Nπ-methyltransferases in ovothiol biosynthesis

We initiated our investigation of SAM-dependent methyltransferases involved in TSI biosynthesis with a comprehensive bioinformatic study. The vast majority of *ovsM* homologs were found to be either fused to *ovoA* or as discrete genes co-encoded with *ovsA*. Unexpectedly, we also discovered a third category within a small family of Campylobacterota that harbor a split version of the *ovoA* gene, with NHISS and methyltransferase domains separated by a large chromosomal distance (Fig. 2A). To the best of our knowledge, standalone 5-thiohistidine *N*-methyltransferases have not been previously reported; we therefore designate these as OvoM. It is tempting to speculate that the monofunctional enzymes OvoM and OvsM may share a more recent common ancestor, possibly arising from a single *ovoA*-gene-splitting event. However, all three classes of TSI-biosynthetic *N*π-methyltransferases (OvoA *C*-terminus, OvoM, and OvsM) are highly similar, with an average pairwise sequence identity of around 50% (Fig. 2B). Furthermore, they appear to be biosynthetically interchangeable as all three efficiently methylate both 5-thioHis and 5-SeHis. Specifically, we recombinantly expressed and purified a member from each category and monitored methyltransferase activity with 5-thioHis or 5-SeHis. Similar conversions were observed with all three enzymes, with slightly higher yields with 5-SeHis, likely resulting from enhanced electron donation into the imidazole ring system rather than an enzymatic preference (Fig. S1).

To gain additional insights, we constructed a phylogenetic tree of the family, which suggests that OvoM and OvsM arose from separate evolutionary events (Fig. 2C). Remarkably, this gene-splitting event seems to have occurred at least three times in their evolution, as evidenced by two distinct clades of OvsM and a single clade of OvoM, all three of which diverged from different regions of the OvoA *C*-terminus phylogeny. The four previously characterized methyltransferases with the highest sequence similarity to OvsM are also included in the phylogenetic tree. Although these enzymes (BorM1, HrsC, MitM, and CyaF)[13-16] likewise methylate N-heterocycles, their similarity to OvsM is surprisingly marginal (Fig. 2C, D). It remains to be seen whether other methyltransferases with intermediate homology catalyze imidazole methylation in other natural products.

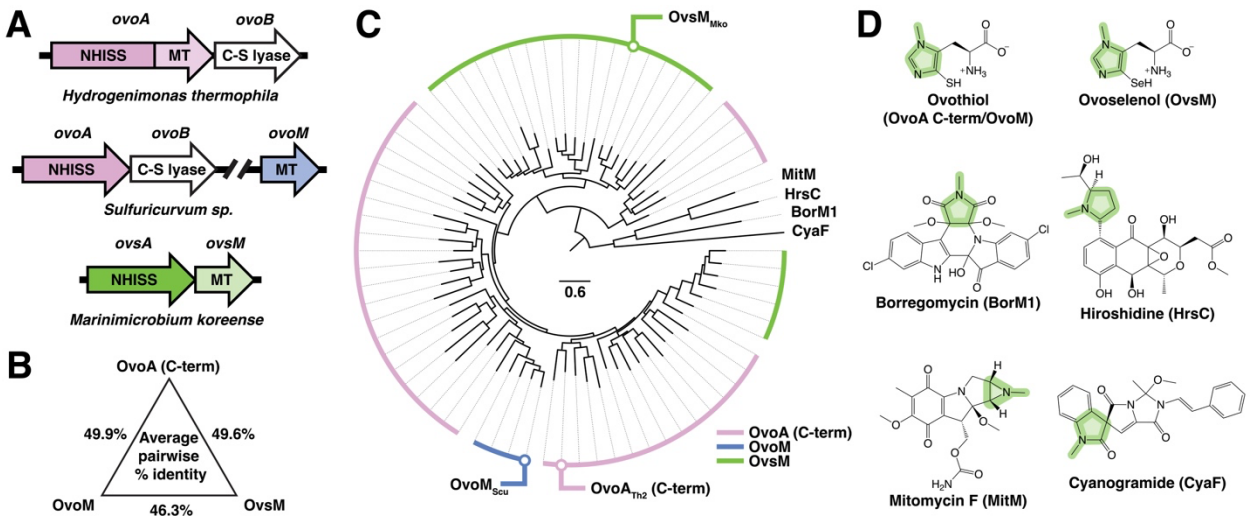

Figure 2. Phylogenetic analysis of SAM-dependent *N*-methyltransferases involved in the biosynthesis of ovoselenol and ovothiol. (**A**) Organization and context of genes encoding three types of TSI-biosynthetic *N*π-methyltransferases (MT): OvoA *C*-terminus, OvoM, and OvsM. (**B**) Average pairwise % sequence identity between the three different MT types. (**C**) Phylogenetic tree, including four distant homologs involved in *N*-methylation of related compounds. Specific proteins analyzed in this study are labeled with circles. (**D**) Products of the MTs displayed in panel C, each of which features a methylated N-heterocycle (shaded green).

Overall architectures of OvsM and OvoM

Given their limited homology to characterized systems, structural insights are crucial to understand the reactivity of the TSI-biosynthetic *N*π-methyltransferases. We, therefore, crystallized representative homologs from *Marinimicrobium koreense* ($OvsM_{Mko}$) and *Sulfuricurvum* sp. isolate STB_99 ($OvoM_{Scu}$). The resultant structures, solved to 1.48 and 2.27 Å resolution, respectively (PDB IDs 9BXH and 9BXM; Table S1, S2), showcase an overall architecture characteristic of the conserved Rossmann fold (Fig. 3A, B). Despite their apparent evolutionary distance (Fig. 2C), their structures are remarkably similar (Fig. S2A), yielding a root-mean-square deviation (RMSD) of 0.69 Å for the peptide backbone (over 825 atoms). In each case, a seven-stranded β-sheet sits at the center of the molecule, surrounded by six major α-helices flanked by two additional two-stranded β-sheets. Typical of class I Rossmann-fold methyltransferases,[17] the β-strand order for the central β-sheet is 3−2−1−4−5−7−6, with the *C*-terminal β-strand oriented antiparallel to the others. The active site is located at the center of the molecule, shaped primarily by loops, α1, and the *C*-terminal region of the central β-sheet. Both models closely align with the

methyltransferase domain of the bifunctional enzyme $OvoA_{Th2}$ (Fig. S2B), displaying only minor differences in secondary structure (Fig. S3). RMSDs of the peptide backbone range from 0.53 Å for $OvoM_{Scu}$ (over 802 atoms) to 0.65 Å for $OvsM_{Mko}$ (over 847 atoms). Their structures also closely align with the carnosine *N*-methyltransferase CARNMT1 (PDB ID 5YF0), yielding backbone RMSDs of 1.89 Å (over 593 atoms) and 2.05 Å (over 585 atoms) for $OvoM_{Scu}$ and $OvsM_{Mko}$, respectively (Fig. S2B). CARNMT1 catalyzes a similar reaction, methylating the imidazole π-nitrogen of its histidine-derived substrate, carnosine.[18] These findings are striking given that CARNMT1 shares virtually no detectable sequence homology with TSI-biosynthetic methyltransferases.

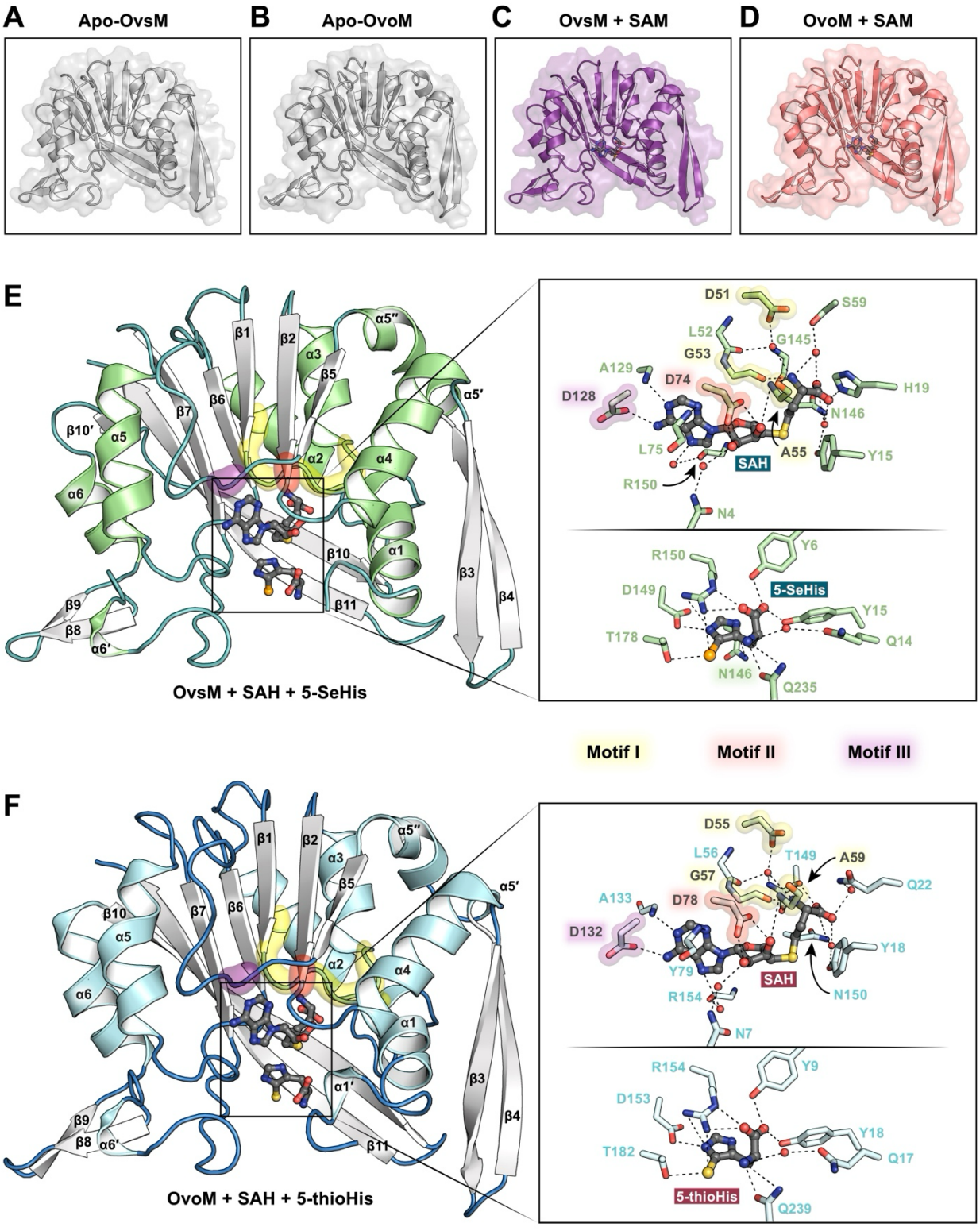

Figure 3. Crystal structures of $OvsM_{Mko}$ and $OvoM_{Scu}$ in various ligand-bound states. Overall structures of (**A**) apo-$OvsM_{Mko}$ (PDB ID 9BXH), (**B**) apo-$OvoM_{Scu}$ (PDB ID 9BXM), (**C**) $OvsM_{Mko}$·SAM complex (PDB ID 9BXJ), (**D**) $OvoM_{Scu}$·SAM complex (PDB ID 9BXL), (**E**) $OvsM_{Mko}$·SAH·5-SeHis

complex (PDB ID 9BXK) and (**F**) $OvoM_{Scu}$·SAH·5-thioHis complex (PDB ID 9BXN). Insets for (E) and (F) show H-bonding interactions for both ligands. Secondary structure elements are labeled, and the ligands are shown in gray sticks. The DxGxAxG sequence (motif I) connecting β1 and α3 is highlighted in yellow, motif II (located at the end of β2) highlighted in red, and motif III (in the loop connecting β5 and β6) highlighted in purple.

Ligand recognition by OvsM and OvoM

To elucidate the active site features that facilitate OvsM- and OvoM-catalyzed methylation at the imidazole π-nitrogen, we subsequently crystallized the enzymes with either the methyl donor SAM or their respective histidine-derived substrate and the co-product *S*-adenosylhomocysteine (SAH). Structures of the $OvsM_{Mko}$·SAM, $OvsM_{Mko}$·SAH·5-SeHis, $OvoM_{Scu}$·SAM, and $OvoM_{Scu}$·SAH·5-thioHis complexes were determined to 1.56, 1.66, 2.09, and 1.70 Å resolution, respectively (PDB IDs 9BXJ, 9BXK, 9BXL, and 9BXN; Fig. 3C-F; S4). Inspection of the binary complexes reveals that the enzymes exhibit conserved SAM-binding motifs typical of nucleoside-binding Rossmann-fold enzymes (Fig. 3E, F).[17, 19, 20] Motif I is characterized by a Gly-rich loop (DxGxAxG) in which the Asp and first Gly residue (D51/D55 and G53/G57 in $OvsM_{Mko}$/$OvoM_{Scu}$) interact with the α-amino moiety of SAM, with the former mediated by a water molecule. The backbone amide of the Ala residue (A55/A59), by contrast, interacts with a ribose hydroxyl group. Motifs II and III consist of acidic residues that interact with the nucleoside region of SAM. The first of these (D74/D78) forms hydrogen (H)-bonds with the ribose hydroxyl groups, while the second (D128/D132) interacts with the adenine ring. Beyond these conserved SAM-binding motifs, a plethora of variable residues located in active site loops and α1 further stabilize SAM through both direct and water-mediated H-bonds (Fig. 3E, F; S5A, B; see SI for details).

The ternary complexes depict the histidine-derived substrates adjacent to SAM, appropriately positioned for methyl group transfer to the π-nitrogen. As with SAM binding, $OvsM_{Mko}$/$OvoM_{Scu}$-mediated recognition of 5-SeHis/5-thioHis primarily involves interactions with active site loops and α1 (Fig. 3E, F; S5C, D), in addition to interactions with a Gln residue (Q235/Q239) from the *C*-terminal β-strand (β11). The 5-SeHis/5-thioHis binding contacts, however, are significantly more conserved compared to SAM binding (Fig. S5). These include Y6/9, Q14/17 (mediated by a water), and Y15/18, which H-bond to the amino acid moiety; as well as

D149/153, which H-bonds to the imidazole ring; and T178/182, which H-bonds to the S/Se atom. Additionally, R150/154 forms multiple H-bonds with the substrate, interacting with the S/Se atom, imidazole ring, and carboxylate moiety. The distinguishing feature of 5-SeHis/5-thioHis binding between the two enzymes lies in the additional interaction between the imidazole side chain of the substrate and N146 in $OvsM_{Mko}$. The analogous Asn from $OvoM_{Scu}$ (N150), while positioned similarly in the active site, is prohibitively distant at approximately 4.3 Å from the closest imidazole nitrogen. Notably, there are no apparent differences that would cause a preference for S vs. Se, consistent with the observation that these enzymes are biosynthetically interchangeable.

Ligand-induced conformational changes in OvsM and OvoM

Superposition of substrate-free $OvsM_{Mko}$ and $OvoM_{Scu}$ with their binary and ternary complexes reveals several structural changes that accompany substrate binding (Fig. 4A, B). In the apo state, electron density was not observed for either of the *N*-termini, indicating they likely sample multiple conformations. Upon binding SAM, these regions undergo stabilization, uniformly orienting toward the active site. This reorganization serves multiple purposes: shaping the solvent-accessible substrate-binding pockets (Fig. 4C, D), and enabling interactions between N4/7 ($OvsM_{Mko}$/$OvoM_{Scu}$) and SAM as well as Y6/9 and 5-SeHis/5-thioHis. In order to accommodate *N*-terminal motion, the side chain of R150/154 shifts away from Y6/9. This reorientation places the side chain parallel with the substrate imidazole upon 5-SeHis/5-thioHis binding, thereby shaping the binding cleft (Fig. 4E, F) and facilitating H-bonding with the substrate. Thus, SAM-binding appears to modulate recognition of the histidine-derived substrate.

This sequential binding model is further confirmed by thermal denaturation analysis using differential scanning calorimetry (DSC), whereby we probed the protein stabilization effects induced by substrate binding. As expected, we observe two progressive increases in the melting temperature of $OvsM_{Mko}$ upon addition of SAH followed by 5-SeHis, but no change upon the addition of 5-SeHis alone, indicating a clear order of binding events (Fig. S6). Examination of the $OvsM_{Mko}$/$OvoM_{Scu}$ ternary complexes reveals that following SAH binding, subsequent interaction with 5-SeHis/5-thioHis is accompanied by a rotameric change in Q235/239 (Fig. 4A, B, G, H).

Y15/18 is also subtly reoriented to optimize the distances for H-bonding with both substrates. In addition to these conserved movements, the $OvoM_{Scu}$ active site undergoes two additional side chain rotations of T149 and T182 upon SAM and 5-thioHis binding, respectively (Fig. 4B).

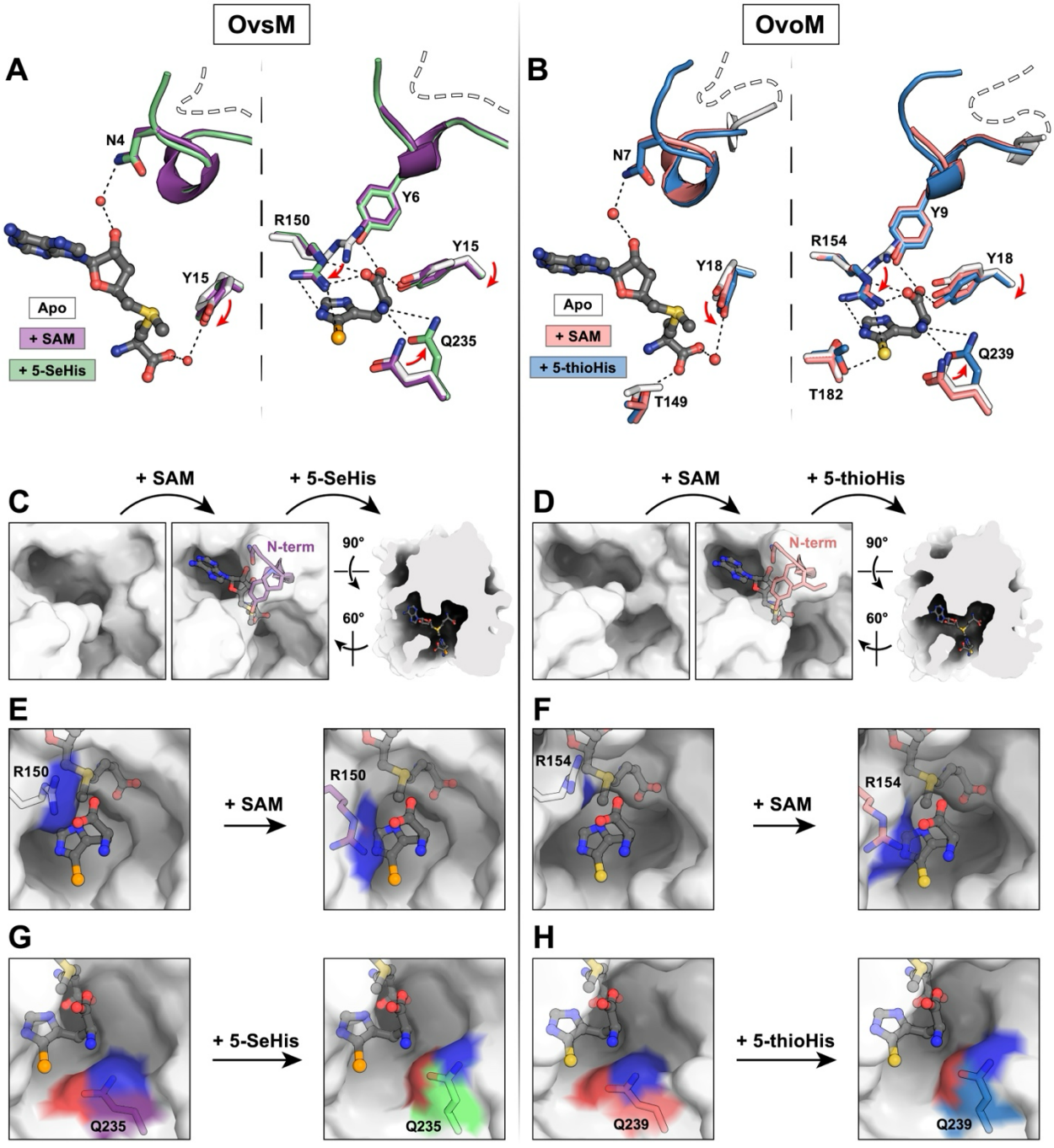

Figure 4. Substrate-induced conformational changes in $OvsM_{Mko}$ and $OvoM_{Scu}$. (**A**) SAM binding (purple) and 5-SeHis/SAH binding (green) stabilize the *N*-terminus of $OvsM_{Mko}$ for ligand

recognition and trigger reorientation of active site residues. (**B**) SAM binding (coral) and 5-thioHis/SAH binding (blue) initiate similar stabilization of the *N*-terminus and side chain movements in $OvoM_{Scu}$. The dashed lines in panels A and B represent the unstructured region of the *N*-terminus in the apo structures. Surface representations of (**C**) $OvsM_{Mko}$ and (**D**) $OvoM_{Scu}$, highlighting the contribution of the *N*-termini to the structure of the substrate-binding site. Shaping of the 5-SeHis/5-thioHis-binding cleft upon SAM-triggered reorientation of (**E**) R150 in $OvsM_{Mko}$ and (**F**) R154 in $OvoM_{Scu}$, and 5-SeHis/5-thioHis-triggered reorientation of (**G**) Q235 in $OvsM_{Mko}$ and (**H**) Q239 in $OvoM_{Scu}$. Note that panels E – H display SAM and 5-SeHis/5-thioHis irrespective of the ligand state, to provide context on how the side chain movements influence the shape of the binding cleft.

Methyltransferase activity in bifunctional, dual-domain OvoA requires domain rearrangement

Comparison with the methyltransferase domain of the bifunctional enzyme $OvoA_{Th2}$ highlights a strikingly similar active site composition (Fig. 5A; S7). This observation suggests that the mode of substrate recognition is likely conserved despite the enzymes' evolutionary separation and modest sequence identities (44-49%; Table S3, S4). A key difference, however, lies in the placement of the *N*-terminal Tyr residue (Y6/9) responsible for H-bonding with the carboxylate of 5-SeHis/5-thioHis in $OvsM_{Mko}$ and $OvoM_{Scu}$. In $OvoA_{Th2}$, the corresponding Tyr residue (Y467) is located distant from the active site in the linker region connecting its two domains. Given that SAM binding to $OvsM_{Mko}$ and $OvoM_{Scu}$ triggers stabilization of their *N*-termini to prime the active site for the histidine-derived substrate, we suspect that $OvoA_{Th2}$ may experience similar SAM-induced conformational rearrangements. Analogous Y467-mediated binding of 5-thioHis, for example, would necessitate rearrangement of the two domains relative to the published crystal structure (Fig. 5B; PDB ID 8KHQ).[12]

Curiously, the *N*-terminus of the chain B $OvoM_{Scu}$ model follows the divergent orientation of the $OvoA_{Th2}$ linker, pointing away from the active site (Fig. 5A; S8). The absence of electron density for 5-thioHis in this monomer supports our analysis above and highlights the essential role of Y9 in substrate recognition. To investigate whether substrate binding by $OvoA_{Th2}$ relies on equivalent interactions, we generated an $OvoA_{Th2}$-Y467F variant for comparison. As anticipated, the mutant displayed markedly diminished catalytic activity (Fig. 5B), supporting this hypothesis and indicating the necessity of domain rearrangement for methyltransferase activity in $OvoA_{Th2}$. Comparable results were obtained for $OvsM_{Mko}$-Y6F (Fig. 5B). The orientations of Y476, R611, and

Q695 in $OvoA_{Th2}$ (Fig. 5A) further substantiate this notion, as these residues closely resemble their counterparts from the apo structures of $OvsM_{Mko}$ and $OvoM_{Scu}$ (Fig. 4A, B). Similar side chain repositioning is therefore necessary to achieve optimal H-bond distances for 5-thioHis binding by the $OvoA_{Th2}$ methyltransferase domain.

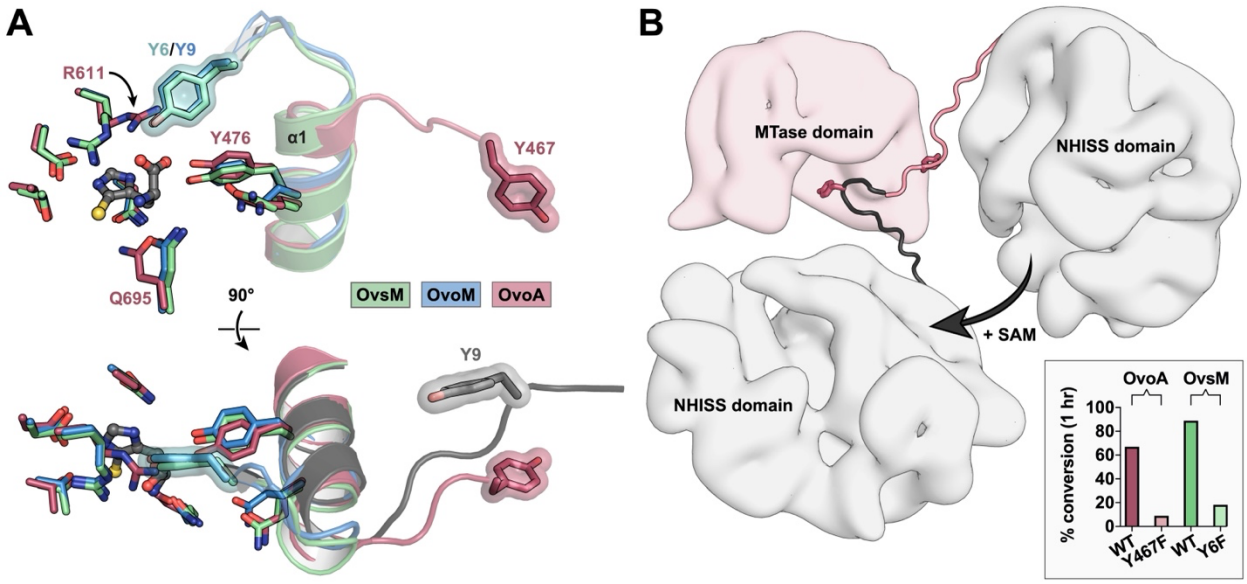

Figure 5. Structural comparison of the methyltransferase domain of $OvoA_{Th2}$ with $OvsM_{Mko}$ and $OvoM_{Scu}$. (**A**) Superposition of the methyltransferase domain of bifunctional $OvoA_{Th2}$ (PDB ID 8KHQ, maroon) with the ternary complexes of $OvsM_{Mko}$ (green) and $OvoM_{Scu}$ (chain A in blue; chain B, exhibiting a catalytically incompetent conformation, in gray). For clarity, chain B is omitted from the top image. (**B**) Hypothetical model for domain rearrangement in $OvoA_{Th2}$ to facilitate Y467-mediated 5-thioHis recognition. Lower right corner: percent conversion of wild-type and mutant $OvoA_{Th2}$ and $OvsM_{Mko}$ ($OvoA_{Th2}$ activity tested using 5-thioHis, $OvsM_{Mko}$ using 5-SeHis).

Histidine Nπ-methyltransferases utilize a catalytic Asp residue for imidazole deprotonation

In addition to providing unique insights into the dynamics associated with substrate binding, our models of the $OvsM_{Mko}$/$OvoM_{Scu}$ reactant complexes allowed us to interrogate the mechanism of these intriguing enzymes. SAM-dependent methyltransferases commonly employ S_N2-like nucleophilic substitution chemistry.[21, 22] Evaluation of our ligand-bound crystal structures supports such a mechanism in OvsM/OvoM, as the imidazole π-nitrogen nucleophilic center is positioned at a distance and orientation optimal for interaction with the electron-deficient methyl

group of SAM. Leveraging these structural insights, we sought to determine whether the enzymes employ base-mediated catalysis, and, if so, to identify the active site base involved. Analysis of the residues proximal to the substrates 5-SeHis and 5-thioHis point to D149/153 and R150/154 as potential candidates.

To assess the role of D149 as the catalytic base in $OvsM_{Mko}$, we mutated it to Asn, attempting to preserve its capacity to H-bond with 5-SeHis while eliminating the negative charge. Subsequent activity assays demonstrated a complete loss of enzymatic activity for the D149N variant (Fig. 6A). Unexpectedly, DSC measurements indicate that this mutation also abolished binding of 5-SeHis (Fig. 6B). We then investigated the catalytic involvement of R150 by generating two additional $OvsM_{Mko}$ variants: R150A and R150Q. Both substitutions resulted in total loss of activity, and the R150Q variant was unable to bind 5-SeHis (Fig. 6A, B). Although we could not decouple the binding and catalytic functions of these residues, based on the positioning of D149/153 in the $OvsM_{Mko}$/$OvoM_{Scu}$ active site relative to the histidine-derived substrate (Fig. 3), we hypothesize that this residue deprotonates the imidazole τ-nitrogen to initiate nucleophilic attack on the methyl group of SAM by the imidazole π-nitrogen (Fig. 6C). By contrast, we suspect that R150/154 fulfills a crucial role in binding 5-SeHis/5-thioHis, rather than in catalysis, by forming multiple H-bonds and contributing to shaping the substrate-binding cleft (Fig. 4A, E).

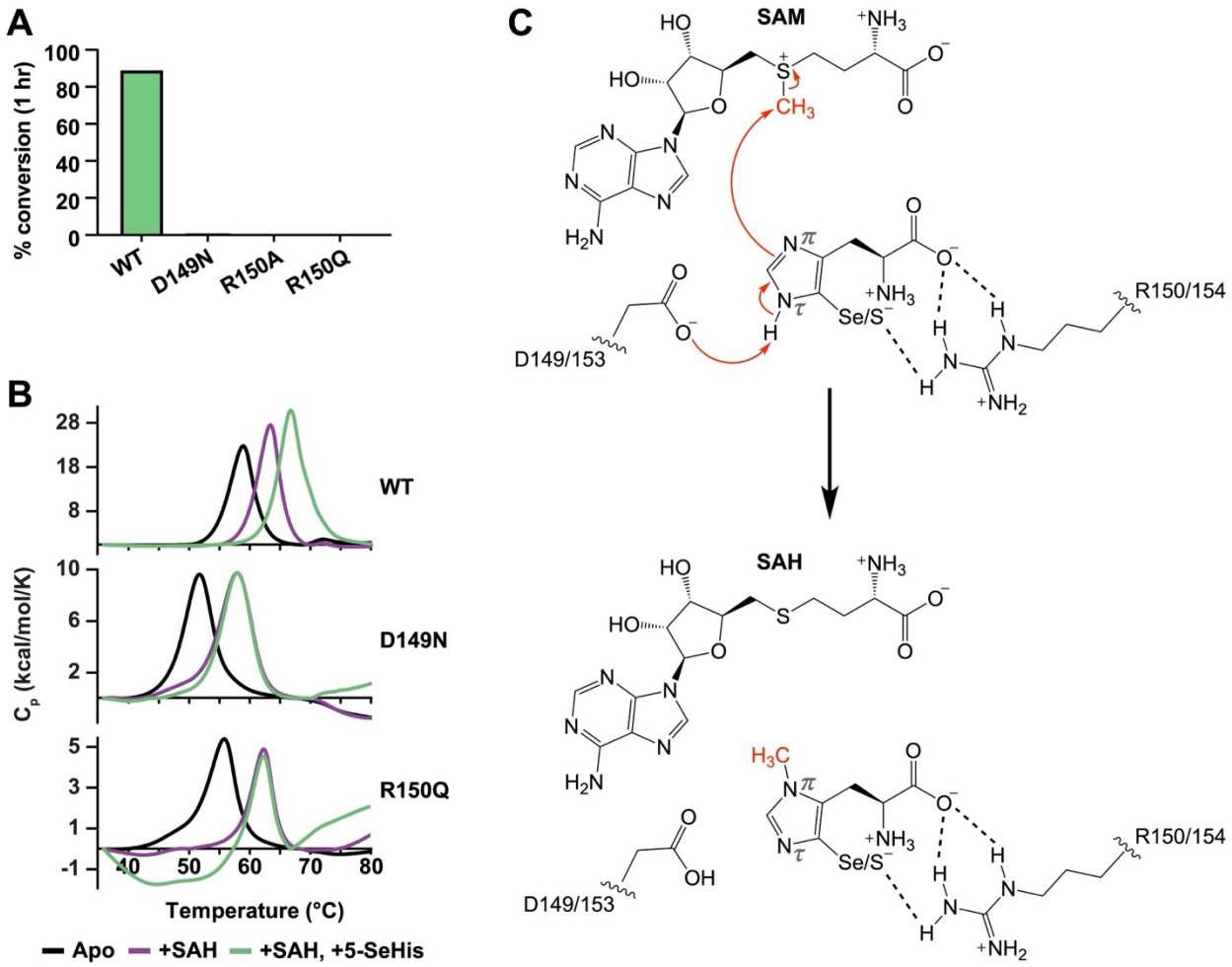

Figure 6. Proposed mechanism of OvsM/OvoM-catalyzed imidazole π-nitrogen methylation. (**A**) Catalytic activity of wild-type and mutant $OvsM_{Mko}$, measured via percent conversion of 5-SeHis. (**B**) Thermal denaturation analysis of wild-type and mutant $OvsM_{Mko}$ using DSC. The protein melting temperature is unaffected by the addition of 5-SeHis in both the D149N and R150Q mutants, indicating that 5-SeHis binding is abolished in these variants. (**C**) S_N2 methyl transfer from SAM to 5-SeHis/5-thioHis. In this model, D149/153 in $OvsM_{Mko}$/$OvoM_{Scu}$ serves as the catalytic base to deprotonate the imidazole τ-nitrogen, initiating nucleophilic attack by the imidazole π-nitrogen on the methyl group of SAM and cleavage of the C–S bond to yield ovoselenol/ovothiol and SAH. Dashed lines represent H-bonds between the substrate and R150/154.

CONCLUSIONS

In this study, we elucidate ligand recognition and reactivity in the *N*π-methyltransferases that catalyze the final step in the biosynthesis of the antioxidants ovothiol and ovoselenol. Through phylogenetic analysis, we uncovered a new subfamily of monofunctional *N*π-methyltransferases, which we have termed OvoM, involved in biosynthesizing ovothiol. Our structural characterization of $OvoM_{Scu}$ and ovoselenol-biosynthetic $OvsM_{Mko}$ reveal that they belong to the Rossmann-fold class of SAM-dependent methyltransferases and exhibit close structural homology to the methyltransferase domain of the bifunctional, ovothiol-biosynthetic enzyme $OvoA_{Th2}$. Analysis of ligand-binding contacts reveals an orchestrated series of substrate-induced conformational movements, the most dramatic of which involves reorientation of the *N*-terminus upon SAM binding to prepare the active site for the histidine-derived substrate. Further examination of the substrate-binding residues offers mechanistic insights into the S_N2-like nucleophilic substitution reaction employed by these enzymes. Analysis of the active site geometry and activity assays on $OvsM_{Mko}$ variants support a mechanism in which D149/153 (in $OvsM_{Mko}$/$OvoM_{Scu}$) serves as the catalytic base for imidazole deprotonation. However, this residue appears to be vital for substrate binding, and these two functionalities could not be fully uncoupled.

Moreover, the structures reported herein suggest that methyltransferase activity by $OvoA_{Th2}$ necessitates significant conformational rearrangement of the NHISS and methyltransferase domains relative to the published crystal structure. In our proposed model, binding of SAM to the methyltransferase domain triggers repositioning of the two domains. The associated reorientation of a key Tyr residue (Y467) located in the linker connecting the two domains facilitates 5-thioHis recognition. Mutagenesis studies support this hypothesis and validate the residue's essential role in methyltransferase activity. Collectively, our findings unveil the molecular basis for *N*π-specific methylation in the ovoselenol and ovothiol biosynthetic pathways, representing a significant advancement in understanding how nature produces these important antioxidants. Furthermore, our identification of a new subfamily of standalone ovothiol-biosynthetic *N*π-methyltransferases, six years after the complete *in vitro* reconstitution

of the ovothiol pathway,[10] highlights the underlying complexity of TSI biosynthesis and suggests that additional aspects may still await discovery.

ASSOCIATED CONTENT

Supporting Information

Detailed description of materials and methods, Tables S1-S4, and Figures S1-S8. (PDF)

Accession Codes

PDB: 9BXH, 9BXJ, 9BXK, 9BXL, 9BXM, 9BXN

ACKNOWLEDGMENTS

We thank the National Science Foundation (Graduate Research Fellowship Program No. 1937971 to K.A.I. and NSF CAREER Award No. 184786 to M.R.S.), the Eli Lilly-Edward C. Taylor Fellowship in Chemistry (to C.M.K.), the George B. Rathmann *51 Fellowship in Chemistry (to M.L.A.), and the National Institutes of Health (grants R01 GM129496 to M.R.S. and R35 GM147557 to K.M.D.) for financial support. We thank Venu Vandavasi at the Princeton University Biophysics Core facility for assistance with DSC experiments. This work is based on research conducted at the Center for High-Energy X-ray Sciences (CHEXS), the Berkeley Center for Structural Biology (BCSB) at the Advanced Light Source (ALS), and the Canadian Light Source (CLS). CHEXS is supported by the NSF (BIO, ENG and MPS Directorates) under award DMR-1829070, and the Macromolecular Diffraction at CHESS facility, which is supported by award 1-P30-GM124166-01A1 from the National Institute of General Medical Sciences (NIGMS), NIH, and by New York State's Empire State Development Corporation. The BCSB is supported in part by the Howard Hughes Medical Institute. The ALS is a DOE Office of Science User Facility under Contract No. DE-AC02-05CH11231. The ALS-ENABLE beamlines are supported in part by the NIH, NIGMS, grant P30 GM124169. The CLS, a national research facility of the University of Saskatchewan, is supported by the Canada Foundation for Innovation, the Natural Sciences and Engineering Research Council, the National Research Council, the Canadian Institutes of Health Research, the Government of Saskatchewan, and the University of Saskatchewan.

REFERENCES

(1) Chen, L.; Zhang, L.; Ye, X.; Deng, Z.; Zhao, C. Ergothioneine and its congeners: anti-ageing mechanisms and pharmacophore biosynthesis. *Protein Cell* **2023**.

(2) Cordell, G. A.; Lamahewage, S. N. S. Ergothioneine, ovothiol A, and selenoneine—histidine-derived, biologically significant, trace global alkaloids. *Molecules* **2022**, *27*, 2673.

(3) Fu, T. T.; Shen, L. Ergothioneine as a natural antioxidant against oxidative stress-related diseases. *Front. Pharmacol.* **2022**, *13*, 850813.

(4) Castellano, I.; Di Tomo, P.; Di Pietro, N.; Mandatori, D.; Pipino, C.; Formoso, G.; Napolitano, A.; Palumbo, A.; Pandolfi, A. Anti-inflammatory activity of marine ovothiol A in an in vitro model of endothelial dysfunction induced by hyperglycemia. *Oxid. Med. Cell Longev.* **2018**, *2018*, 2087373.

(5) Brancaccio, M.; D'Argenio, G.; Lembo, V.; Palumbo, A.; Castellano, I. Antifibrotic effect of marine ovothiol in an in vivo model of liver fibrosis. *Oxid. Med. Cell Longev.* **2018**, *2018*, 5045734.

(6) Miyata, M.; Matsushita, K.; Shindo, R.; Shimokawa, Y.; Sugiura, Y.; Yamashita, M. Selenoneine ameliorates hepatocellular injury and hepatic steatosis in a mouse model of NAFLD. *Nutrients* **2020**, *12* (6).

(7) Kayrouz, C. M.; Ireland, K. A.; Ying, V.; Davis, K. M.; Seyedsayamdost, M. R. Discovery of the selenium-containing antioxidant ovoselenol derived from convergent evolution. *Nat. Chem.* **2024**.

(8) Kayrouz, C. M.; Huang, J.; Hauser, N.; Seyedsayamdost, M. R. Biosynthesis of selenium-containing small molecules in diverse microorganisms. *Nature* **2022**, *610* (7930), 199-204.

(9) Braunshausen, A.; Seebeck, F. P. Identification and characterization of the first ovothiol biosynthetic enzyme. *J. Am. Chem. Soc.* **2011**, *133* (6), 1757-1759.

(10) Naowarojna, N.; Huang, P.; Cai, Y.; Song, H.; Wu, L.; Cheng, R.; Li, Y.; Wang, S.; Lyu, H.; Zhang, L.; et al. In vitro reconstitution of the remaining steps in ovothiol A biosynthesis: C—S lyase and methyltransferase reactions. *Org. Lett.* **2018**, *20* (17), 5427-5430.

(11) Ireland, K. A.; Kayrouz, C. M.; Huang, J.; Seyedsayamdost, M. R.; Davis, K. M. Structural characterization and ligand-induced conformational changes of SenB, a Se-glycosyltransferase involved in selenoneine biosynthesis. *Biochemistry* **2023**, *62* (23), 3337-3342.

(12) Wang, X.; Hu, S.; Wang, J.; Zhang, T.; Ye, K.; Wen, A.; Zhu, G.; Vegas, A.; Zhang, L.; Yan, W.; et al. Biochemical and structural characterization of OvoA(Th2): a mononuclear nonheme iron enzyme from Hydrogenimonas thermophila for ovothiol biosynthesis. *ACS Catal.* **2023**, *13* (23), 15417-15426.

(13) Chang, F. Y.; Brady, S. F. Discovery of indolotryptoline antiproliferative agents by homology-guided metagenomic screening. *Proc. Natl. Acad. Sci. U.S.A.* **2013**, *110* (7), 2478-2483.

(14) Moon, K.; Xu, F.; Zhang, C.; Seyedsayamdost, M. R. Bioactivity-HiTES unveils cryptic antibiotics encoded in Actinomycete bacteria. *ACS Chem. Biol.* **2019**, *14* (4), 767-774.

(15) Varoglu, M.; Mao, Y.; Sherman, D. H. Mapping the mitomycin biosynthetic pathway by functional analysis of the MitM aziridine N-methyltransferase. *J. Am. Chem. Soc.* **2001**, *123*, 6712-6713.

(16) Zhu, Y.; Zhang, Q.; Fang, C.; Zhang, Y.; Ma, L.; Liu, Z.; Zhai, S.; Peng, J.; Zhang, L.; Zhu, W.; et al. Refactoring the concise biosynthetic pathway of cyanogramide unveils spirooxindole formation catalyzed by a P450 enzyme. *Angew. Chem. Int. Ed. Engl.* **2020**, *59* (33), 14065-14069.

(17) Kozbial, P. Z.; Mushegian, A. R. Natural history of S-adenosylmethionine-binding proteins. *BMC Struct. Biol.* **2005**, *5* (19).

(18) Cao, R.; Zhang, X.; Liu, X.; Li, Y.; Li, H. Molecular basis for histidine N1 position-specific methylation by CARNMT1. *Cell Research* **2018**, *28* (4), 494-496.
(19) Martin, J. L.; McMillan, F. M. SAM (dependent) I AM: the S-adenosylmethionine-dependent methyltransferase fold. *Curr. Opin. Struct. Biol.* **2002**, *12* (6), 783-793.
(20) Gana, R.; Rao, S.; Huang, J.; Wu, C.; Vasudevan, S. Structural and functional studies of S-adenosyl-L-methionine binding proteins: a ligand-centric approach. *BMC Struct. Biol.* **2013**, *13* (6).
(21) O'Hagan, D.; Schmidberger, J. W. Enzymes that catalyse SN2 reaction mechanisms. *Nat. Prod. Rep.* **2010**, *27* (6), 900-918.
(22) Liscombe, D. K.; Louie, G. V.; Noel, J. P. Architectures, mechanisms and molecular evolution of natural product methyltransferases. *Nat. Prod. Rep.* **2012**, *29* (10), 1238-1250.

For Table of Contents Only

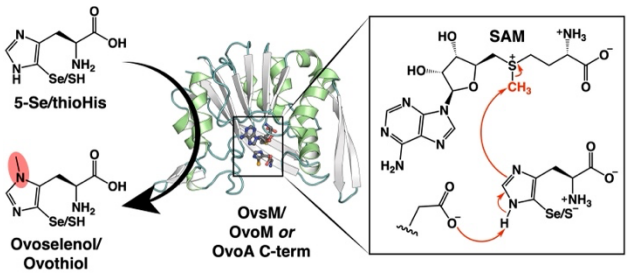

Synopsis: The *N*π-methyltransferases that produce the antioxidants ovoselenol and ovothiol feature a series of conserved conformational movements and appear to use an Asp base for nucleophilic substitution.